

# The effect of an embedded cathode on lithium migration in mortar specimens

Lourdes M. S. Souza <sup>1,2</sup>, Rob B. Polder <sup>1,3</sup>, Oguzhan Çopuroğlu <sup>1</sup>

<sup>1</sup> Faculty of Civil Engineering and Geosciences, Delft University of Technology, the Netherlands

<sup>2</sup> Tecgraf Institute, Pontifical Catholic University of Rio de Janeiro, Brazil

<sup>3</sup> TNO Technical Sciences/Structural Reliability, Delft, the Netherlands

The currently available treatment techniques for concrete structures affected by alkali-silica reaction (ASR) are limited and electrochemical lithium migration has been proposed as an alternative. Lithium compounds have shown to have beneficial effects on ASR expansion when used as admixtures to fresh concrete. During the electrochemical treatment, lithium ions are transported into concrete (or mortar) by the action of an electrical field. The same principle is behind well-established techniques such as electrochemical chloride extraction (ECE). Like during ECE treatments, the reinforcement may be used as cathode during electrochemical lithium migration.

In this paper, an investigation of the use of an embedded cathode during electrochemical lithium migration is presented. Mortar specimens were cast with embedded titanium meshes, which worked as cathodes. Results showed that potassium and sodium ions accumulated in the region around the embedded mesh and, under the tested conditions, few lithium ions reached that area. The accumulation of sodium and potassium is an undesirable side effect that increases the pH, which may possibly induce further ASR development, if not enough lithium ions reach the area.

*Keywords: Alkali-silica reaction, migration, lithium, cathode*

## 1 Introduction

The currently available intervention methods for concrete structures diagnosed with alkali-silica reaction (ASR) are limited and, in many cases, not effective (Rajabipour et al., 2015; Nixon and Sims, 2015). In this framework, lithium-based treatments have been proposed as possible mitigation methods.

The use of lithium-based admixture is a well-established preventive method against ASR in new concrete structures (McCoy and Caldwell, 1951; Stark et al., 1993; Hooper et al., 2004). Lithium ions have been generally acknowledged to alter the reaction mechanism or the formed ASR product (Ramyar et al., 2004; Feng et al., 2005; Rajabipour et al., 2015). In existing structures, however, the incorporation of lithium-based admixtures to the fresh concrete is no longer possible. In this case, lithium ions need to be driven into the concrete, in order to reach areas where the reaction takes place.

Different methods of lithium impregnation such as topical application, vacuum impregnation, submitting to wet-dry cycles and immersion, have been investigated and results have shown that, in those cases, lithium penetration was limited in both content and penetration depth (Stark et al., 1993; Thomas and Stokes, 2004; Folliard et al., 2008; Santos Silva et al., 2008). In contrast, lithium electrochemical migration has provided better lithium impregnation, in both penetration depth and content and it has shown to be the most suitable among the investigated techniques (Thomas and Stokes, 2004; Santos Silva et al., 2008). Electrochemical lithium migration is a technique in which an electric field is used to drive lithium ions into concrete (or cementitious material). The same principle is applied in treatments such as electrochemical chloride extraction (ECE). In fact, it was first proposed as a modification of the ECE procedure, in order to treat structures which not only suffered from chloride induced corrosion, but were also affected by ASR (Page, 1992).

Electrochemical lithium migration has been studied as a technique to drive lithium ions and mitigate ASR development by various authors (e.g. Thomas and Stokes (2004); Santos Silva et al. (2008); Whitmore and Abbott (2000); Ueda et al. (2006); Pacheco and Polder (2010); Liu et al. (2011); Ueda et al. (2014, 2015); Souza et al. (2015a); Souza (2016); Souza et al. (2017)). However, there is no agreement on its effectiveness. In those studies, the position of the negative electrode (cathode) varied. In some investigations, a concrete or mortar specimen was placed in a two-chamber type of set-up and the cathode was placed externally to the specimen in a relatively large volume of solution. In this case, not only lithium ions impregnated the specimen, but also sodium and potassium ions were removed from the pore solution of the specimens and entered the cathode solution. In other studies, as it is the case with ECE treatment of actual structures, the rebar (or an embedded electrode) was used as cathode. The use of embedded rebar as cathode might alter the lithium migration process and lead to undesirable side effects, such as the accumulation of alkali ions in the region around it (which may possibly induce further

ASR development). In this paper, the effects of the use of an embedded cathode during electrochemical lithium migration are discussed.

## 2 Experimental program

### 2.1 Materials and specimen preparation

Mortar cylinders, with a diameter of 98 mm and a height of 60 mm, were cast with a titanium mesh at 10 mm from one of the surfaces, as shown in Figure 1. The mesh was embedded to represent the situation when a reinforcement bar would be used as cathode in a structure under treatment. The mortar mixture had a water to cement ratio (w/c) of 0.5 and fine aggregate to cement proportion of 3:1. Ordinary Portland cement type CEM I 42.5 N was used and its chemical composition is shown in Table 1. The fine aggregate was a CEN standard sand with  $D_{max}$  of 2 mm (according to NEN-EN 196-1 (2005)), which is assumed to be nonreactive, and the water used in the mixture was deionized. The mixing procedure followed the standard EN 196 1:2005 (NEN-EN 196-1, 2005).

The flow value of the mortar mixture, measured by the flow table test (NEN-EN 12350-5, 2009), was 270 mm and the air void content, obtained with an air-entrainment-meter (NEN-EN 12350-7, 2009), was 1.0%. After casting, the specimens were cured in a fog room ( $20.0 \pm 2.0$  °C and R.H. of  $96 \pm 2\%$ ) for 36 days prior to testing.



Figure 1: Specimen with embedded titanium mesh. The wire coming out of the specimen on the left is from the embedded mesh.

Table 1: Cement composition, wt. % of cement

CaO	SiO <sub>2</sub>	Al <sub>2</sub> O <sub>3</sub>	Fe <sub>2</sub> O <sub>3</sub>	SO <sub>3</sub>	MgO	P <sub>2</sub> O <sub>5</sub>	K <sub>2</sub> O	TiO <sub>2</sub>	Na <sub>2</sub> O	Other	L.O.I. <sup>1</sup>
65.00	18.33	4.42	3.38	3.01	2.02	0.57	0.46	0.37	0.28	0.53	1.60

<sup>1</sup> L.O.I.: loss on ignition

## 2.2 Methods

Lithium migration testing was performed in a set-up similar to the one described by ASTM 1202 (ASTM-C1202-05, 2005). As shown in the scheme of Figure 2, each specimen was positioned between two chambers, one with lithium solution (270 ml) and the other remained empty, working only as support for the specimen. For these experiments, a 4.9 M LiOH solution was chosen as the anolyte, in order to avoid acidification of the solution and deterioration of the specimen, as observed in previous work (Souza et al., 2015a; Souza, 2016). The chamber with electrolyte received a titanium mesh with iridium/tantalum oxide coating (with mesh diamond dimensions of about 4 x 8 mm) that worked as anode and an embedded titanium mesh (with approximate diamond dimensions of 20 x 60 mm) in the specimen was used as cathode. Two types of cells were used. They were identical, except for the presence of ventilation holes in the ring around the specimen in cells type I, (Figure 3) whereas there were no ventilation holes in cells type II.

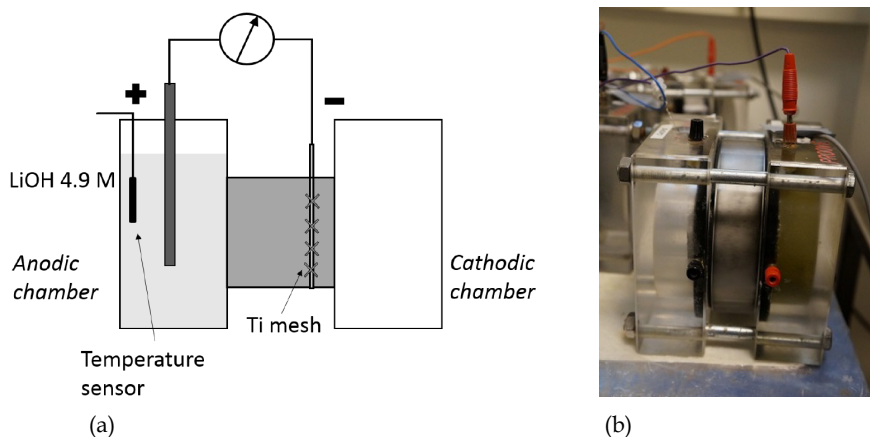


Figure 2: Diagram of the experimental set-up (a) and experimental set-up (b)

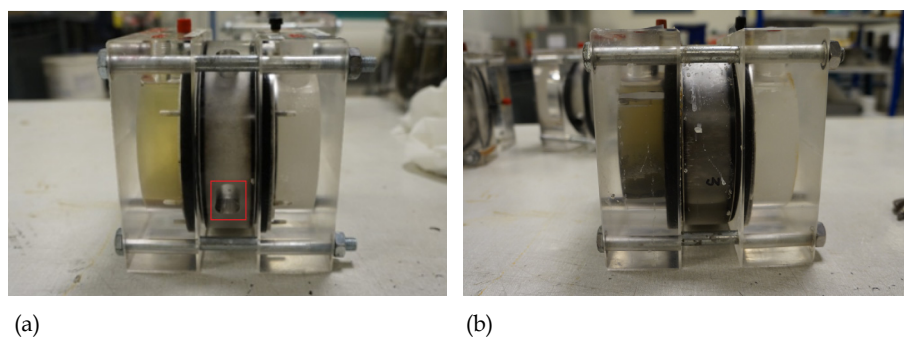


Figure 3: The two types of migration cells – type I, with ventilation holes in the rings around the specimen (a) and type II, without ventilation holes (b) (Souza et al., 2015b)

The experiments lasted four or eight weeks and the applied voltage was 15 or 25 V (electric field of c. 0.3 or 0.5 V/mm). These voltage values were chosen in order to avoid the very high currents and temperatures observed in previous work (Souza, 2016), where similar specimens were submitted to 40 V. Testing was carried out in a climate controlled laboratory, at  $20.0 \pm 2.0$  °C and R.H. of  $50 \pm 5\%$ .

Passing current and anolyte temperature were continuously recorded by a data logger. Current density values were calculated in relation to the surface area of the specimens. The specimen electrical resistance and the pH of the anolyte solutions were measured once a week. The specimen electrical resistance was measured with a LCR-meter in resistance mode at 120 Hz. The resistivity values ( $\rho$ ,  $\Omega\text{m}$ ) were calculated using the following equation, assuming that the resistance outside the specimen was negligible (Polder, 2001):

$$\rho = \frac{RA}{L} \quad (1)$$

where  $R$  is the electrical resistance of the specimen ( $\Omega$ ),  $A$  is the surface area of the specimen ( $\text{m}^2$ ) and  $L$  is the distance between the anodic surface and the embedded mesh (m).

The pH of the anolyte solutions was obtained with pH test strips (range 7.5 - 14). The anolyte solutions were sampled once a week and analysed by inductively coupled plasma optical emission spectroscopy (ICP-OES), in order to obtain sodium, potassium, lithium and calcium concentrations. The anolyte chambers had their solution levels completed with deionized water before sampling, to avoid the influence of evaporation on the concentration values. After the migration tests, images from the specimens were made in an X-ray computed tomography scanner, in order to check for debonding of the mesh. The images were made in a macro CT-scanner similar to the ones used for medical applications. The resolution on the horizontal plane (the plane of each slice) was 0.3 mm and the resolution in the vertical direction was 1.0 mm.

Finally, the specimens were cut into slices of approximately 5.0 mm, which were ground in a micro ball mill. The powder (10-20 g) was dissolved in 100 ml of boiling 3.0 M  $\text{HNO}_3$  solution. The solution was then filtered and the filtrate was washed with four parts of 10 ml of 1.0 M  $\text{HNO}_3$ . The final clear solutions were then analysed by ICP-OES for lithium, sodium and potassium contents.

### 3 Results and discussion

Current density plots are shown in Figure 4. The cells exhibited rapid increase in current density in the first hours and reached a maximum value in less than 12 hours, similarly to what was observed in other studies (Pacheco and Polder, 2010; Souza, 2016). After that, the current density dropped steadily until about day 30, when it stabilized until the end of the experiment (in the case of the cells tested for eight weeks).

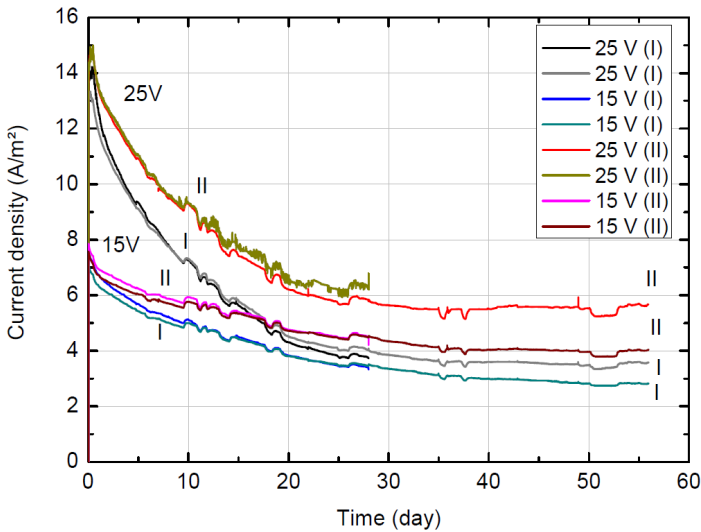


Figure 4: Current density plots in the experiments with embedded cathode

Among specimens tested in the same type of cell, the ones tested under 25 V presented higher current density than those under 15 V, as expected. When comparing the cells under the same level of voltage, it can be noted that cells in the set-up type II presented higher current density than those in the set-up type I - and the difference was more pronounced when the applied voltage was higher.

It is worth noting that specimens under 25 V had current densities above 10 A/m<sup>2</sup> for the first days, which subsequently dropped to lower values, whereas for the cells under 15 V, that level was not reached. The maximum current density for those cells was around 8 A/m<sup>2</sup>. Early studies in the 1980s have shown that the application of current densities above 10 A/m<sup>2</sup> during electrochemical treatments, such as chloride extraction, led to concrete deterioration, see overview in (Bertolini et al., 2013). Later studies, a.o. discussed

in (Polder and Van den Hondel, 2002), suggest that current densities significantly higher than  $1 \text{ A/m}^2$ , applied for typically four weeks, could reduce steel-concrete bond.

Figure 5 shows the anolyte temperatures, which were all below  $30 \text{ }^\circ\text{C}$ . From day 14 until day 20, the cell LiOH 4.9 M (8 w. 25V I) did not have its anolyte temperature measured due to problems with the temperature sensor. The temperature of the anolytes follow the same trend as the current density plots. The cells under 25 V had the highest temperatures and, for the same voltage level, the set-ups type I presented slightly lower values. This happened most likely due to the presence of ventilation holes in the perspex ring around the specimen. Lower temperatures led to higher resistivity values and, finally, to lower current densities. Table 2 shows the passing charges. As expected, a higher voltage and a longer period of testing led to a higher charge. In addition, specimens tested in set-ups type II had higher passing charge than the ones tested in cells type I.

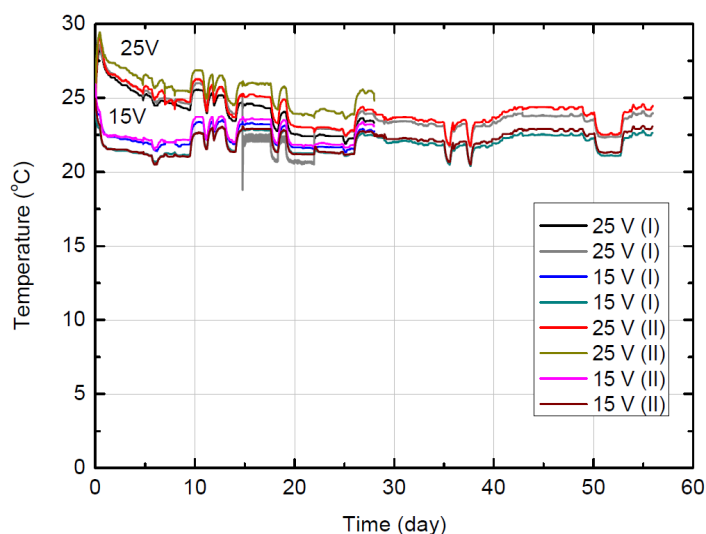


Figure 5: Anolyte temperature plots in the experiments with embedded cathode

Electrical resistivity values during the experiment are shown in Figure 6. Table 3 shows the average values between replicates at different moments during the experiments. Initially, the specimens presented average resistivity of  $35 \pm 1 \text{ } \Omega\cdot\text{m}$ . The specimens tested in cells type I (either for four or eight weeks) presented increasing resistivity until the end of the experiment. The ones tested in set-up type II had increasing values for the first four weeks and then their resistivity stabilized until the end of the eight weeks' testing period.

Table 2: Passing charges for the experiments with embedded cathode

Cell	Charge (kC)
LiOH 4.9 M 4w 25V (I)	123
LiOH 4.9 M 8w 25V (I)	186
LiOH 4.9 M 4w 15V (I)	88
LiOH 4.9 M 8w 15V (I)	138
LiOH 4.9 M 4w 25V (II)	159
LiOH 4.9 M 8w 25V (II)	253
LiOH 4.9 M 4w 15V (II)	103
LiOH 4.9 M 8w 15V (II)	172

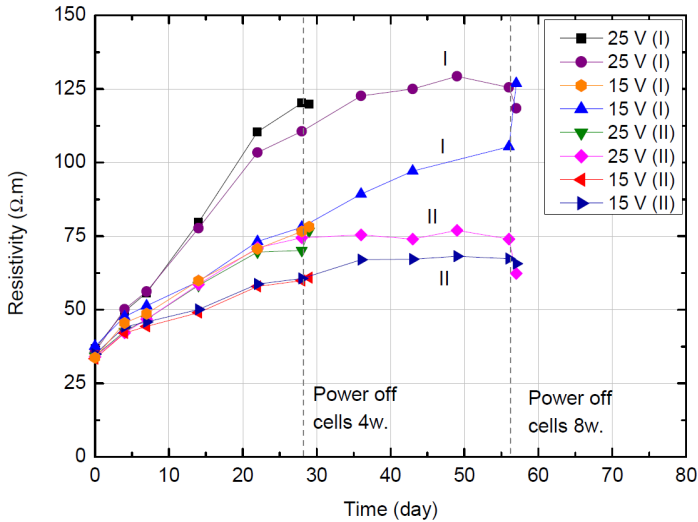


Figure 6: Cell resistivity behaviour during experiments with embedded cathode

The difference in behaviour between specimens in different types of cells is clearly visible in Figure 6 and is expressed in the variations between replicates (Table 3). For the same level of applied voltage, specimens tested in set-ups type I presented greater increments in resistivity than the ones tested in cells type II.

Within the same type of set-up, the cells that received a higher voltage had higher resistivity by the end of the experiment. At the end of the tests, the current was turned off and resistance was measured after 24 hours. Interestingly, the resistivities did not return to

Table 3: Average resistivity values at different moments of the experiments with embedded cathode

	LiOH 4.9 M (4 w. 25 V)		LiOH 4.9 M (4 w. 15 V)	
	Av. ( $\Omega$ .m)	CV (%)	Av. ( $\Omega$ .m)	CV (%)
Initial	36	4	34	1
Middle (14 days)	69	16	55	10
End	95	26	68	12
After 24 h	98	22	70	13
	LiOH 4.9 M (8 w. 25 V)		LiOH 4.9 M (8 w. 15 V)	
	Av. ( $\Omega$ .m)	CV (%)	Av. ( $\Omega$ .m)	CV (%)
Initial	35	2	36	4
Middle (28 days)	93	20	69	13
End	100	26	86	22
After 24 h	90	31	96	32

the initial values, indicating that the variations during the experiment were not a mere effect of temperature. This indicates that there were, in fact, non-reversible (in the short term) changes in the pore structure and /or in the pore solution composition. One possibility could be that the production of  $H_2$  on the titanium mesh in the specimens, due to cathodic reaction:



led to development of pressure that resulted in local debonding. In order to check for development of cracking around the mesh, the specimens were analysed by computerized tomography (CT). Figure 7 shows CT scan images from the region around the mesh of the specimen LiOH 4.9 M (8w. 25 V). No debonding or cracking were detected at the resolution used in this analysis. Even though microcracks smaller than the used resolution may have been formed, resistance increase would be caused by large scale debonding or cracking at the cathode plane, and these were not observed in the CT scan images.

The pH of the anolyte solution of all cells remained 14 throughout the test, due to the very high pH of the initial solution, even though hydroxyl ions were consumed at the anode, according to the reaction:



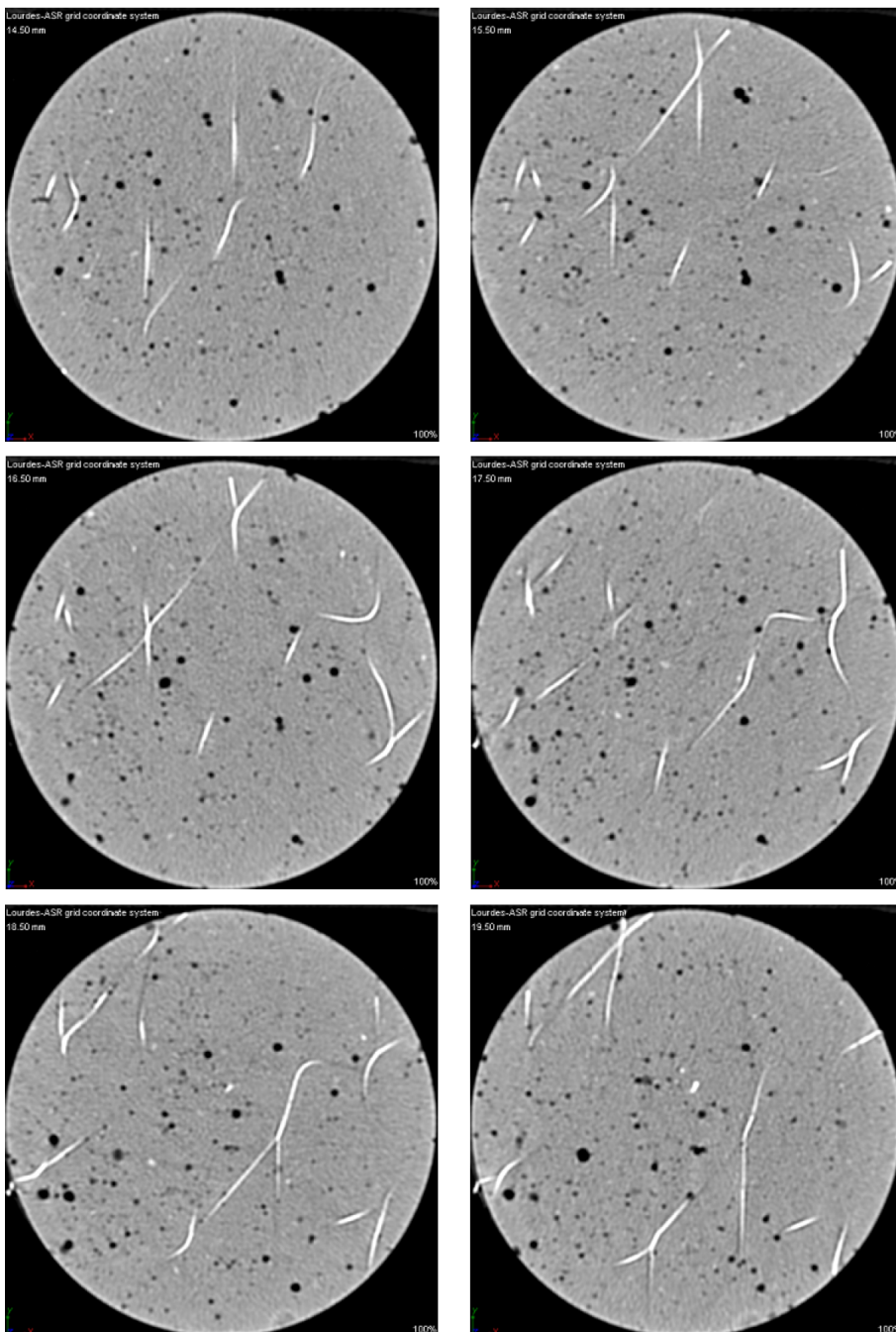


Figure 7: Images obtained by computerized tomography of the region around the titanium mesh in specimen LiOH 4.9 M (8w. 25 V). The light areas are the wires of the mesh. No debonding or cracking can be detected.

Figure 8 presents the chemical composition of the analyte solutions during the experiment. Sodium, potassium and calcium ions leached from the specimen during the first couple of days and reached constant levels throughout the tests (Figure 8 (a), (b) and (c)). There is no correlation between passing charges and final level of those concentrations. Lithium ions left the analyte into the specimen, as expected (Figure 8 (d)). Overall, the specimens with the highest passing charges are the ones with the lowest final lithium concentrations in the analyte, as expected.

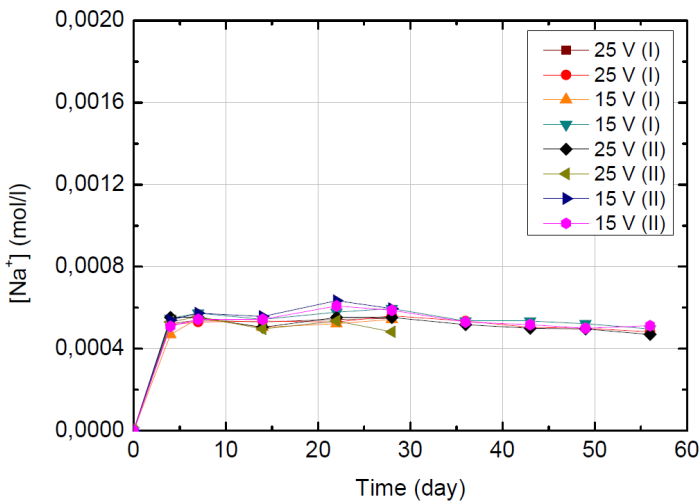


Figure 8a: Sodium concentrations in analyte solutions during experiments with embedded cathode

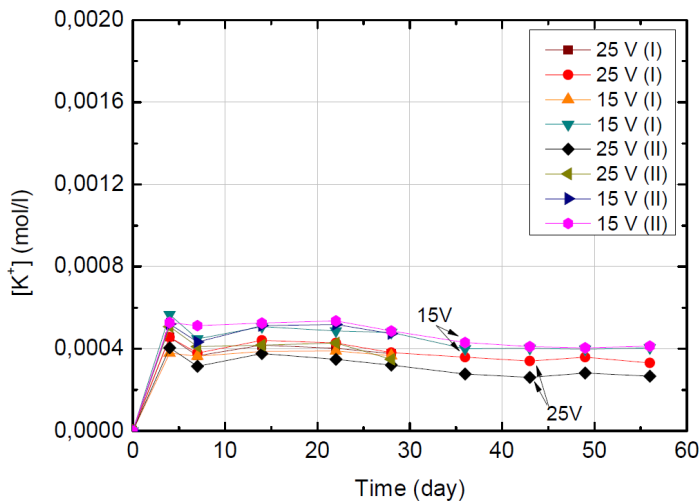


Figure 8b: Potassium concentrations in analyte solutions during experiments with embedded cathode

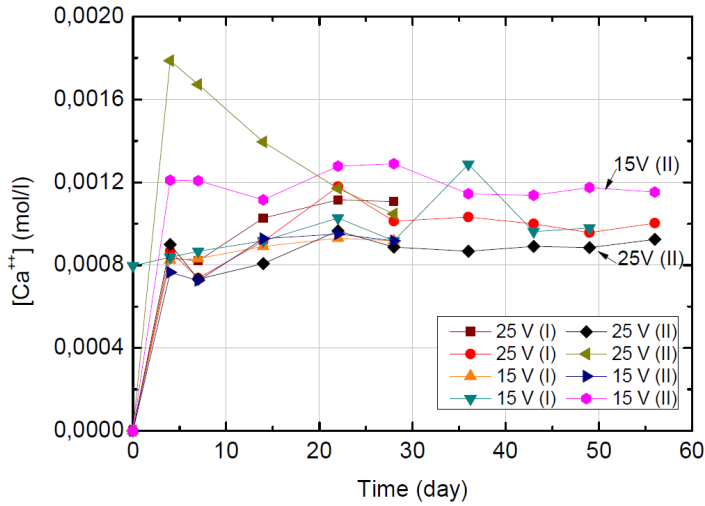


Figure 8c: Calcium concentrations in anolyte solutions during experiments with embedded cathode

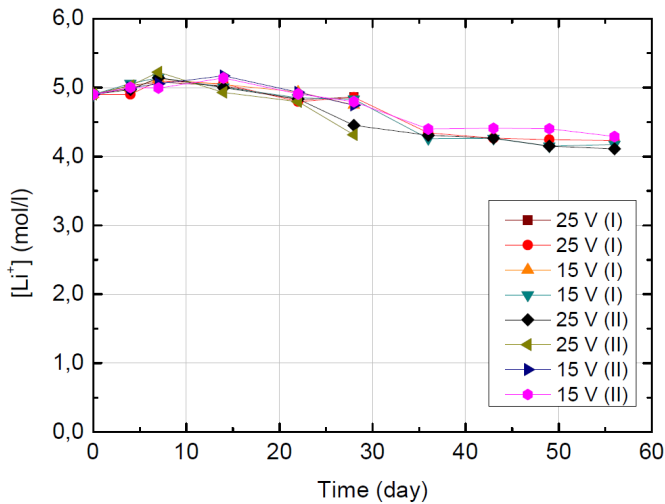


Figure 8d: Lithium concentrations in anolyte solutions during experiments with embedded cathode

Total sodium and potassium content profiles in the specimen can be seen in Figure 9. As expected, sodium and potassium ions were attracted by the cathode and concentrated in the area around it. Overall, the contents in the region until 35-40 mm from the anode are quite low. They probably represent sodium and potassium that is bound to solid phases. The sodium and potassium contents are similar to the ones found in previous experiments (Souza et al., 2015a; Souza, 2016) with similar mortar specimens but with external cathodes, in which most (if not all) free sodium and potassium ions were removed from the pore solution. Therefore, it is likely that in the present experiments most free sodium and potassium left the region closer to the anode and accumulated in the region around

the cathode. In addition, the specimens with the highest passing charge had profiles shifted towards the cathode.

As sodium and potassium ions accumulate around the cathode, hydroxyl ions produced by the cathodic reaction are likely to accumulate in that region, in order to electrically balance the positive charge of the alkali ions. In the case of the treatment of ASR affected concrete using the reinforcement as cathode, the increase in alkali and hydroxyl concentrations in that area is likely to locally induce further formation of ASR gel (if enough reactive silica is still present in the system). In fact, Bentivegna et al. (2011)

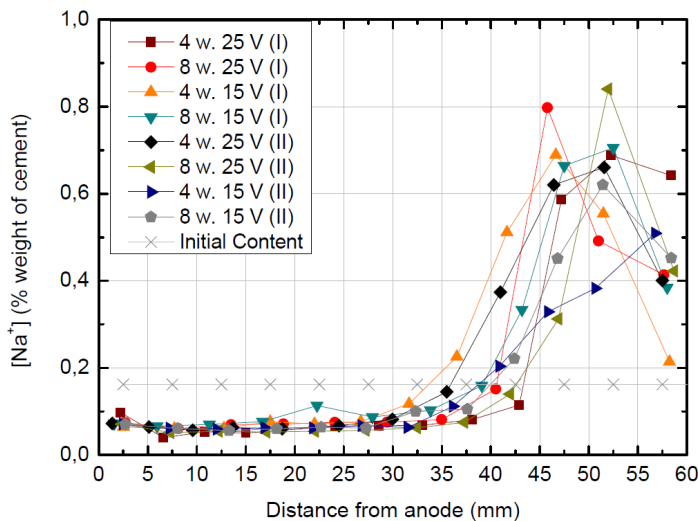


Figure 9a: Sodium contents in the specimens tested with embedded cathode. The mesh is situated at 50 mm from the anode.

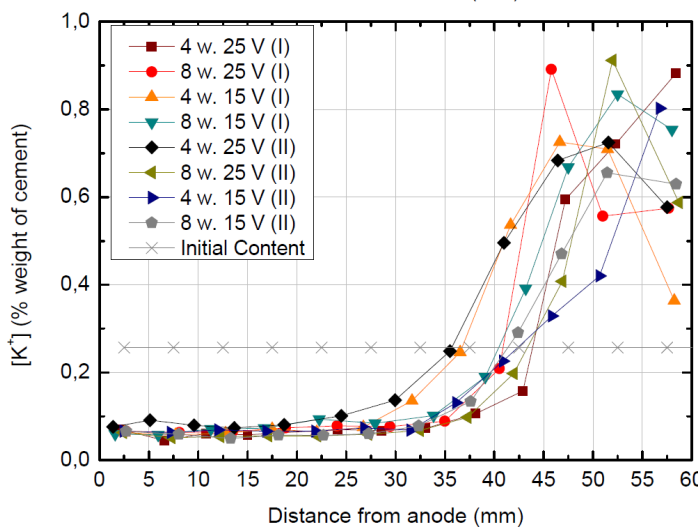


Figure 9b: Potassium contents in the specimens tested with embedded cathode. The mesh is situated at 50 mm from the anode.

mentioned that the alkali accumulation around the reinforcement combined with the lack of lithium ion in that area after treatment were probably the cause for the remaining expansive behaviour. In their experiments, treated columns had expansion levels similar or greater than the untreated ones. Thus, the accumulation of sodium and potassium near the cathode is a potentially dangerous side effect, if not enough lithium ions reach that area, in order to mitigate further expansion (Souza et al., 2017).

Total lithium content profiles are shown in Figure 10. The specimens with the highest passing charges are the ones in which lithium ions were able to reach deeper layers. In fact, the average lithium content in the specimens, shown in Table 4, can be correlated to the passing charges. Nevertheless, in most specimens, lithium ions did not reach deeper layers.

Lithium to alkali molar ratios ( $\frac{[Li]}{[Na+K]}$ ) throughout the specimens can be seen Figure 11.

No specimen had  $\frac{[Li]}{[Na+K]}$  above 1.0 in all regions. In fact, most specimens only reached that value in the first 25-35 mm from the anode.

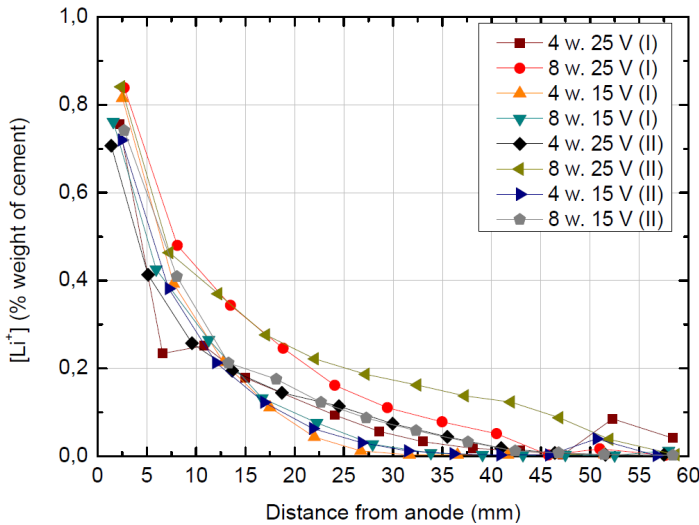


Figure 10: Lithium profiles in the specimens tested with embedded cathode. The mesh is situated at 50 mm from the anode.

In previous work (Souza et al., 2015a; Souza, 2016), migration experiments were performed with similar specimens and the same anolyte solution, but with external electrodes (both anode and cathode in a relatively large volume of solution). In those tests, lithium only reached the cathodic chamber once most of (if not all) free sodium and potassium were removed from the pore solution throughout the specimens. This could indicate that, in the case when the cathode is embedded, the region around it would hardly be impregnated by

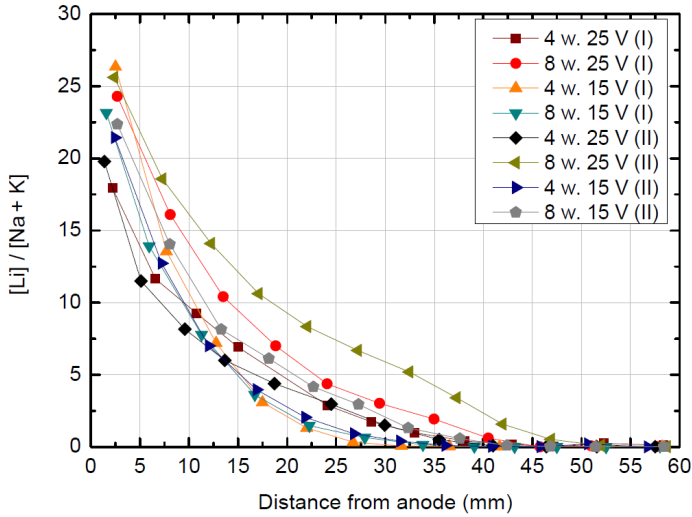


Figure 11: Lithium to alkalis molar ratio in the specimen tested with embedded cathode. The mesh is situated at 50 mm from the anode.

Table 4: Average lithium content in specimens after testing

Specimen	Average Li (%wt. of cement)
LiOH 4.9M 4w 25V (I)	0.13
LiOH 4.9M 8w 25V (I)	0.20
LiOH 4.9M 4w 15V (I)	0.13
LiOH 4.9M 8w 15V (I)	0.13
LiOH 4.9M 4w 25V (II)	0.13
LiOH 4.9M 8w 25V (II)	0.23
LiOH 4.9M 4w 15V (II)	0.13
LiOH 4.9M 8w 15V (II)	0.15

lithium. After all, in this case, sodium and potassium ions are not removed from the pore solution around the embedded cathode. This could be a limiting factor to the treatment.

Indeed, during the migration tests with embedded cathodes, sodium and potassium ions accumulated in the region around the cathode and few lithium ions reached that area (Figures 9 and 10). However, these experiments were performed under 15 or 25 V, whereas the ones with external electrodes were conducted under 40 V. Therefore, the reason why not so many lithium ions could reach the cathodic region in the embedded case could possibly be the limited passing charge (due to lower applied voltage). It is likely that, as long as there would be current in the system and enough lithium in the anolyte, lithium

ions would be able to be transported towards the cathode and accumulate in the region around it. Electrical equilibrium would be achieved with the hydroxyls produced by the cathodic reaction. Therefore, it is possible that lithium ions would reach the cathodic area during longer migration experiments.

## 4 Conclusions

In this paper, the effect of the use of embedded cathodes on lithium migration was studied. The following conclusions can be drawn.

- As expected, cells under 25 V presented higher current density and passing charge than the cells under 15 V. In addition, the ventilation holes in the rings around the specimens influenced the results - cells with no ventilation holes presented higher passing charge, probably due to higher temperatures and consequently lower mortar resistivity.
- The resistivity values 24 h after the application of current of all specimens were significantly higher than the initial ones, indicating that non-reversible changes (at least on the short term) to the pore structure and/or pore solution composition may have taken place. Debonding of the titanium mesh was not observed in images obtained by computerized tomography, so macroscopic delamination was not the cause. Hydrogen gas formation at the cathode is also not a likely explanation, as the period of 24 hours after discontinuing current flow is expected to be sufficient to let hydrogen gas escape.
- Sodium and potassium ions accumulated in the region close to the titanium mesh. Moreover, very few or no lithium ions arrived in that region. The lack of lithium ions in the cathodic region was probably caused by the passing charge. If higher voltage was applied or testing lasted longer, it is possible that lithium ions would have arrived to that region.

### *Acknowledgments*

This work was supported by Dutch Technology Foundation (STW), Sika Technology AG, BAM Infraconsult BV, Rijkswaterstaat, TNO Delft, Van Nieuwpoort Grint en Zand B.V. and TCKI - Stichting Technisch Centrum voor de Keramische Industrie (STW project 10971: "Modelling, non-destructive testing and Li-based remediation of deleterious Alkali-Silica Reaction in concrete structures").

The authors gratefully acknowledge CorrPRE Engineering for providing the titanium anodes.

## References

- ASTM-C1202-05 (2005). Standard test method for electrical indication of concrete's ability to resist chloride ion penetration.
- Bentivegna, A., Giannini, E., and Folliard, K. (2011). Use of electrochemical migration to mitigate alkali-silica reaction in large scale concrete structures. *Concrete Solutions*, Dresden, Eds. M. Grantham, V. Mechtcherine, U. Schneck, Taylor and Francis, London, 123-131.
- Bertolini, L., Elsener, B., Pedferri, P., Redaelli, E., and Polder, R. B. (2013). *Corrosion of steel in concrete: prevention, diagnosis, repair*. John Wiley & Sons, 2nd edition.
- Feng, X., Thomas, M., Bremner, T., Balcom, B., and Folliard, K. (2005). Studies on lithium salts to mitigate ASR-induced expansion in new concrete: a critical review. *Cement and Concrete Research*, 35(9):1789-1796.
- Folliard, K. J., Thomas, M. D., Ideker, J. H., East, B., and Fournier, B. (2008). Case studies of treating asr-affected structures with lithium nitrate. In *Proceedings of the 13th International Conference on Alkali-Aggregate Reaction in Concrete*, pages 90-99.
- Hooper, R. L., Nixon, P. J., and Thomas, M. D. (2004). Considerations when specifying lithium admixtures to mitigate the risk of ASR. In *Proc. 12 th Int. Conf. on Alkali-Aggregate Reaction in Concrete*, pages 554-563.
- Liu, C.-C., Wang, W.-C., and Lee, C. (2011). Behavior of cations in mortar under accelerated lithium migration technique controlled by a constant voltage. *Journal of Marine Science and Technology*, 19(1):26-34.
- McCoy, W. and Caldwell, A. (1951). New approach to inhibiting alkali-aggregate expansion. In *ACI Journal Proceedings*, volume 47. ACI.
- NEN-EN 12350-5 (2009). Testing fresh concrete - part 5: Flow table test.
- NEN-EN 12350-7 (2009). Testing fresh concrete - part 7: Air content - pressure methods.
- NEN-EN 196-1 (2005). Methods of testing cement - part 1: Determination of strength.
- Nixon, P. J. and Sims, I. (2015). *RILEM Recommendations for the Prevention of Damage by Alkali-Aggregate Reactions in New Concrete Structures: State-of-the-Art Report of the RILEM Technical Committee 219-ACS*, volume 17. Springer.
- Pacheco, J. and Polder, R. B. (2010). Preliminary study of electrochemical lithium migration into cementitious mortar. In *2nd International Symposium on Service Life Design for Infrastructures*, pages 1093-1100. RILEM Publications SARL.
- Page, C. (1992). Interfacial effects of electrochemical protection methods applied to steel in chloride-containing concrete. In *Proceedings of International Conference on Rehabilitation of Concrete Structures*, pages 179-187.

- Polder, R. and Van den Hondel, A. (2002). Laboratory investigation of electro-chemical chloride extraction from concrete with penetrated chloride. *HERON*, 47:211–220.
- Polder, R. B. (2001). Test methods for on site measurement of resistivity of concrete - a RILEM TC -154 technical recommendation. *Construction and Building Materials*, 15(2):125–131.
- Rajabipour, F., Giannini, E., Dunant, C., Ideker, J. H., and Thomas, M. D. (2015). Alkalisilica reaction: Current understanding of the reaction mechanisms and the knowledge gaps. *Cement and Concrete Research*, 76:130–146.
- Ramyar, K., Çopuroğlu, O., Andıç, Ö., and Fraaij, A. (2004). Comparison of alkali-silica reaction products of fly-ash-or lithium-salt-bearing mortar under long-term accelerated curing. *Cement and Concrete Research*, 34(7):1179–1183.
- Santos Silva, A., Salta, M., Melo Jorge, M., Rodrigues, M., and Cristino, A. (2008). Research on the suppression expansion due to ASR. Effect of coatings and lithium nitrate. In *Proceedings of the 13th International Conference on Alkali-Aggregate Reaction in Concrete*.
- Souza, L. M., Polder, R. B., and Çopuroğlu, O. (2015a). Influence of anolyte on lithium migration in concrete. In *Durability of Reinforced Concrete from Composition to Protection*, pages 27–34. Springer.
- Souza, L. M., Polder, R. B., and Çopuroğlu, O. (2017). Lithium migration in a two-chamber set-up as treatment against expansion due to alkali-silica reaction. *Construction and Building Materials*, 134:324–335.
- Souza, L. M. S. (2016). *Electrochemical lithium migration to mitigate alkali-silica reaction in existing concrete structures*. PhD thesis, Delft University of Technology.
- Souza, L. M. S., Polder, R. B., and Çopuroğlu, O. (2015b). Lithium migration in mortar specimens with embedded cathode. In *Concrete Repair, Rehabilitation and Retrofitting IV: Proceedings of the 4th International Conference on Concrete Repair, Rehabilitation and Retrofitting (ICCRRR-4)*, 5-7 October 2015, Leipzig, Germany, page 39. CRC Press.
- Stark, D., Morgan, B., and Okamoto, P. (1993). Eliminating or minimizing alkali-silica reactivity. Technical Report SHRP-C-343, Strategic Highway Research Program.
- Thomas, M. and Stokes, D. (2004). Lithium impregnation of ASR-affected concrete: preliminary studies. In *Proceedings of the 12th International Conference on Alkali-Aggregate Reaction in Concrete*, pages 659–667.
- Ueda, T., Baba, Y., and Nanasawa, A. (2013). Penetration of lithium into ASR affected concrete due to electro-osmosis of lithium carbonate solution. *Construction and Building Materials*, 39:113–118.

- Ueda, T., Kushida, J., Tsukagoshi, M., and Nanasawa, A. (2014). Influence of temperature on electrochemical remedial measures and complex deterioration due to chloride attack and ASR. *Construction and Building Materials*, 67:81–87.
- Ueda, T., Nanasawa, A., and Tsukagoshi, M. (2015). Influence of electrochemical lithium penetration from various kinds of lithium solution on ASR expansion of concrete. In *Proceedings of the 4th International Conference on Concrete Repair, Rehabilitation and Retrofitting*. CRC Press.
- Ueda, T., Yoshida, Y., Yamaguchi, K., and Ashida, M. (2006). Electrochemical migration of lithium ions into hardened concrete and ASR expansion after treatment. *Proceedings of structural faults & repair-2006*.
- Whitmore, D. and Abbott, S. (2000). Use of an applied electric field to drive lithium ions into alkali-silica reactive structures. In *Proceedings, 11th International Conference on Alkali-Aggregate Reaction*, pages 1089–1098.

